Ceramics International 46 (2020) 353–364

Contents lists available at ScienceDirect

Ceramics International

journal homepage: www.elsevier.com/locate/ceramint

Superior biological performance and osteoinductive activity of Si-containing bioactive bone regeneration particles for alveolar bone reconstruction

Zhe Mao[a,1], Yifan Gu[b,1], Jing Zhang[c], Will Wenmiao Shu[d], Yingqiu Cui[a,*], Tao Xu[e,f,**]

[a] Department of Oral and Maxillofacial Surgery, Guangzhou Women and Children's Medical Center, Guangzhou Medical University, Guangzhou, 510120, China
[b] Department of Orthopaedics, The First Affiliated Hospital of Anhui University of Traditional Chinese Medicine, Hefei, 230031, China
[c] Medprin Regenerative Medical Technologies Co., Ltd, Guangzhou, 510663, China
[d] Department of Biomedical Engineering, University of Strathclyde, Wolfson Centre, 106 Rottenrow, Glasgow, G4 0NW, United Kingdom
[e] Department of Mechanical Engineering, Biomanufacturing Center, Tsinghua University, Beijing, 100084, China
[f] Department of Precision Medicine and Healthcare, Tsinghua-Berkeley Shenzhen Institute, Shenzhen, 518055, China

ARTICLE INFO

Keywords:
Bioactive bone graft
Alveolar bone reconstruction
Osteoconduction
Osteoinduction

ABSTRACT

Bone grafting materials for repair of alveolar bone deficits have improved markedly in recent years, increasing the applicability and success of oral implantology. The long-term success rate of dental implant surgery is strongly dependent on the quality and stability of residual bone tissue. Therefore, reconstruction of resorbed alveolar bone is a challenge for clinicians. In the present study, we have developed bioactive bone regeneration particles (BRPs) using amorphous calcium phosphate and 58S bioglass as raw materials. The structural characteristics, biocompatibility, and osteoinductivity of these BRPs were compared to commercially available bovine spongy bone (BSB) without organic components. X-ray diffractometry (XRD) and scanning electron microscopy (SEM) showed that BRPs were composed of β-tricalcium phosphate (β-TCP) and calcium silicate in the form of hexagonal crystals, while BSB was mainly hydroxyapatite (HA) arranged in orderly nano-sized crystals. The viability of human bone marrow mesenchymal stem cells (hBMSCs) cultured in BRP-containing medium was roughly equal to that of hBMSCs in control medium. Moreover, hBMSCs in BRP medium exhibited greater proliferation rates, substrate attachment, alkaline phosphatase (ALP) activity, alizarin red staining intensity, and expression levels of osteogenic-related genes (COL-I, OCN, Runx-2, ALP, BSP) than hBMSCs in BSB medium, indicating the superior osteoinductivity of BRPs. Silicon ions released from BRPs during cell culture were crucial for these enhanced biological properties. BRPs also demonstrated superior osteoconduction and osteoinduction properties for bone defect repair, suggesting promise for alveolar bone repair surgery.

1. Introduction

In recent years, widely application of bone grafting materials in the defect of alveolar bone has been improved due to the development of the oral implantology. The long-term success rate of dental implant surgery depends to a great extent on sufficient alveolar bone mass around the implant and integration between implant and circumjacent natural bone. Therefore, implant surgery has higher requirements for ambient bone tissue. The irreversible process of alveolar bone absorption can be easily caused by tooth loss, improper routine exodontia, bad prosthesis or other factors, which leads to decreased alveolar bone width and height, creating challenges for predictable implant placement [1]. Moreover, insufficient bone volume in the implant area as well as reduces the success rate of dental implant surgery [2,3]. In order to expand the application scope and success of oral implantology, many researchers have sought to develop improved bone repair materials for regenerative treatment of bone deficiency.

Reconstruction of resorbed alveolar bone is a challenge for clinicians and a variety of bone repair materials has been applied in the clinic. Autogenous bone, xenogenic bone and synthetic bone have usually used in oral surgeries such as immediate or delayed augmentation around implants, extraction sockets preservation after tooth extractions, alveolar ridge augmentation or reconstruction, etc [4–7]. Each of these materials has unique advantages and disadvantages.

* Corresponding author. Department of Oral and Maxillofacial Surgery, Guangzhou Women and Children's Medical Center, Guangzhou Medical University, Guangzhou, 510623, China.
** Corresponding author. Department of Mechanical Engineering, Biomanufacturing Center, Tsinghua University, Beijing, 100084, China.
E-mail addresses: gzhtwang@163.com (Y. Cui), taoxu@mail.tsinghua.edu.cn (T. Xu).
[1] These authors contributed equally.

https://doi.org/10.1016/j.ceramint.2019.08.269
Received 26 July 2019; Received in revised form 26 August 2019; Accepted 27 August 2019
Available online 29 August 2019

Autogenous bone, obtained from intraoral or extraoral donor sites, has been extensively used due to its osteoconductive and osteoinductive properties [8]. However, its high absorption rate usually compromise the clinical outcomes. Indeed, both animal and human studies indicate that around half of the autologous bone graft is absorbed within four months [9,10]. Xenogeneic bone has extensive sources and its bone structure is similar to natural bone. In addition, xenogeneic bone generally allows good osteoconduction, but implantation may result in immunological rejection or non-healing of alveolar bone defect. Synthetic bone grafts have good biocompatibility and biodegradability and have a certain ability of osteoconduction. However, both xenogeneic and synthetic bones lack sufficient osteoinductive capacity, resulting in slower new bone formation. Given the advantages of synthetic bone (reduce risk of rejection, potentially unlimited supply), it would be of substantial clinical value to develop a synthetic bone material with better osteoinductive function.

Currently, the xenogeneic bone most widely used in clinical practice originates from bovine spongy bone (BSB), which is mainly composed of hydroxyapatite (HA) without organic matter. The porous nature of BSB allows for the growth of new bone tissue and provides a suitable scaffold for bone tissue regeneration. However, little bovine spongy bone can degrade in the defect site, and it remains in the form of foreign matter for a very long time. The synthetic bone commonly used in clinical practice is composed mainly of hydroxyapatite, calcium phosphate (TCP) or other materials. It has been proved that TCP has demonstrated good biocompatibility and appropriate biodegradability, which is essential for adhesion and proliferation of bone cells [11]. Further, its chemical composition is similar to that of natural bone tissue, so there are no obvious inflammatory reactions after implantation.

Silicon (Si)-containing biomaterials have achieved widely attention due to the released Si ions have the function of inducing osteogenesis and angiogenesis, promoting the repair of bone tissue and the formation of new blood vessels [12,13]. In the study of Wang [14,15], silicate-apatite composite layers precipitated on titanium rods demonstrated increased osteoblastic proliferation and differentiation in vitro, and are promising as coatings on external fixation pins for decreasing the pin tract infection rate in vivo. Bioglass (BG), one of the Si-containing biomaterials, has also attracted much attention as a potential regenerative material due to its biological activity and biocompatibility [16,17]. Studies have shown strong ion exchange between bioglass and bone tissue, so it can directly participate in the metabolism and regeneration of new bone [18]. It can ultimately induce the growth of new bone in the surface of bioglass material. The Ca, P, and Si ions released from BG can help to form a strong chemical bond at the interface with bone tissue, improving the interface integration between the material and new bone [19]. However, pure bioglass has a relatively faster degradation rate that does not match the growth rate of new bone. A potential solution is the development of bioglass-containing composite materials that retain the aforementioned advantages of bioglass but with slower degradation kinetics.

In this study, we combined β-tricalcium phosphate (β-TCP) with 58S bioglass (60 mol% SiO_2-36 mol% CaO-4 mol% P_2O_5) to adjust the overall osteogenic properties and degradation rate. Subsequently, a bulk precursor of the bone repair material required for oral implantation was prepared through freeze-lyophilization, followed by fragmentation and sintering to obtain bone repair particles with osteogenic activity. The physicochemical properties and biosafety of the material were tested and compared with the bovine spongy bone particles (BSBs) commonly used in clinical practice. In vitro cell experiments and animal implantation experiments were used to evaluate the osteogenic properties of the materials in detail.

2. Materials and methods

2.1. Preparation of amorphous calcium phosphate powder

Amorphous calcium phosphate (ACP) powder was synthesized by chemical precipitation method using calcium nitrate ($Ca(NO_3)_2{\cdot}4H_2O$, 1.0 mol/L) and diammonium phosphate ($(NH_4)_2HPO_4$, 0.8 mol/L). $(NH_4)_2HPO_4$ solution was added into $Ca(NO_3)_2{\cdot}4H_2O$ solution slowly at room temperature with Ca/P ratio of 1.5, and ammonia water was added into the mixed solution to control the pH value between 6.5–7, yielding a white precipitate. After stirring for 5 h and aging for 24 h, the white precipitate was harvested, washed with deionized water and absolute ethyl alcohol, and oven dried. Final ACP powder with particle size of less than 100 μm was recovered by sieving.

2.2. Preparation of bioglass powder

58S bioglass was prepared using sol-gel method. Tetraethyl orthosilicate (TEOS) and triethyl phosphate (TEP) were hydrolyzed in 2 mol/L nitric acid to form sol. And then calcium nitrate ($Ca(NO_3)_2{\cdot}4H_2O$) was added into the sol under stirring condition until it was completely dissolved. After aging for 48 h, drying for 5 days, heat treatment at 650 °C for 3 h, and final grinding and sieving, bioglass powder (BG) with a particle size of not more than 100 μm was obtained.

All the chemical reagents used in the synthesis of ACP powder and 58S bioglass powder were of AR grade and were commercially obtained from Shanghai Aladdin Bio-Chem Technology Co., China.

2.3. Preparation of active bone regeneration particles

Polycaprolactone (weight-average molecular weight of 80,000) was dissolved in dioxane under 90 °C water bath to obtain 20 wt% of a polycaprolactone viscous solution. ACP and BG powders were added to the polycaprolactone solution at a ACP to BG mass ratio of 3:2 and total powder concentration in solution of 0.8 g/mL. A planetary ball mill was used to mix the mixture to form homogeneous slurry. The uniformly homogenized slurry was then subjected to a freeze-lyophilization process to obtain a desired bulk precursor. The irregular particles, which were obtained through fragmentation treatment, were sintered at 1250 °C for 2 h and sieved to obtain bioactive bone regeneration particles (BRPs) with a particle size range of 0.25–1 mm.

2.4. Phase composition and micromorphology

Commercially available bovine spongy bone (BSB) was used as control material. The BRPs and BSBs were ground into fine powders, and the phase compositions of BRP and BSB powders were analyzed by X-ray diffractometer (XRD; X'Pert PRO; PANalytical Co., the Netherlands) using CuKα radiation (λ = 1.5418 Å) with 2θ from 10° to 70°. The scanning step size is 0.016° and final data were analyzed using X'Pert HighScore software.

The surface micromorphology of BRPs and BSBs was observed using a scanning electron microscope (SEM; Nova NanoSEM 430, FEI, USA). Briefly, BRPs and BSBs were pasted on conductive tape and coated with a thin layer of gold. Accelerating voltage of 15 kV was used for image acquisition.

2.5. In vitro cell experiment

2.5.1. Preparation of BRP and BSB culture media

In this experiment, the effects of BRP and BSB on the proliferation and osteogenic differentiation of human bone marrow mesenchymal stem cells (hBMSCs; HUXMA-01001, Cyagen, USA) were systematically investigated using BRP- and BSB -containing culture media. The BRP and BSB particles were sealed in centrifuge tubes and sterilized by ^{60}Co γ-irradiation with 20 kGy. Then complete culture medium (or

Table 1
Primers used for RT-PCR analysis.

Target gene	Forward primer sequences (5′-3′)	Reverse primer sequences(3′-5′)
GAPDH	AGAAAAACCTGCCAAATATGATGAC	TGGGTGTCGCTGTTGAAGTC
Runx-2	AGATGATGACACTGCCACCTCTG	GGGATGAAATGCTTGGGAACT
Collagen-I	CAGCCGCTTCACCTACAGC	TTTTGTATTCAATCACTGTCTTGCC
OCN	TCACACTCCTCGCCCTATTG	ACAGTCCGGATTGAGCTCAC
ALP	ACATTCCCACGTCTTCACATTT	AGACATTCTCTCGTTCACCGCC
BSP	ATGGCCTGTGCTTTCTCAATG	GGATAAAAGTAGGCATGCTTG

osteogenic induction medium) at a particle weight-to-medium ratio of 0.2 g/mL was added into sample tubes. A real-time extraction process at 37 °C was carried out. Briefly, the BRP and BSB soaking mediums were completely collected and transferred separately to the relevant cell culture plates every other day. The medium of the samples was renewed with fresh medium immediately after removal.

The calcium and silicon ion contents in the collected media were detected. Briefly, the collected media were digestion using concentrated nitric acid and the ions contents were tested using inductively coupled plasma-atomic emission spectrometry (ICP-AES, Optimal 5300DV, PerkinElmer, USA). Three replicate samples were prepared for each treatment group at each time point.

2.5.2. Cytotoxicity and cell proliferation assays

Prior to cell seeding, hBMSCs were maintained in culture flasks under 95% humidity and a 5% CO_2 atmosphere at 37 °C. Only hBMSCs at passage 6 were used for experiments. Briefly, cells were digested with 0.25% trypsin/EDTA (Gibco, 25200-056), resuspended in complete culture medium (No.HUXMA-90011, Cyagen, USA), and seeded at the indicated density. The medium was exchanged with BSB or BRP medium as indicated after 4 h, which was then changed every second day.

The cytotoxicity of BRPs was analyzed according to the protocol of ISO 10993-5. Cells were resuspended and seeded on 48-well plates at 5×10^3 cell/well (500 μL cell suspension/well). The complete culture medium was completely changed with BRP medium (prepared as described) 4 h later. Cells cultured in complete culture medium were used as a negative control. Four duplicate samples were prepared for each treatment group. After 24 h of culture, the cytotoxicity of BRP was examined using a Cell Counting Kit-8 (CCK-8 kit) according to the manufacturer's protocol (Dojindo, Japan). Briefly, the medium was removed and 250 μL of CCK-8 working solution was added to each well. After 1 h, 100 μL of the resulting orange-yellow supernatant in each well was transferred to 96-well plates, and the optical density (OD) value read at 405 nm using an enzyme-linked immune sorbent assay (ELISA) plate reader. The same CCK-8 kit was used to monitor cell proliferation. Briefly, the assay was conducted after 1, 3, and 7 days of culture. Four replicated were prepared for each treatment group.

For cell viability assays, cells were seed as described, incubated for 48 h in BRP or BSB medium and stained using the Viability/Cytotoxicity Assay Kit for Animal Live & Dead Cells (Calcein-AM & Ethidium homodimer-III; Biotium, NO.30002, USA). Briefly, cells were washed 3 times with PBS to remove the residual medium, stained with fluorescence staining working solution for 45 min away from light. The stained cells were washed 3 times with PBS, observed with an inverted fluorescence microscope (Eclipse Ti2–U, Nikon, Japan), and the fluorescence images were taken with a charge-coupled device (CCD) camera.

The alkaline phosphatase (ALP) activity of hBMSCs cultured in BRP and BSB osteogenic induction medium was evaluated by both ALP staining and a quantitative biochemical assay. After 7 and 14 days in culture (initial seeding density of 5×10^4 per well in 48-well plate), cells were stained using BCIP/NBT substrate solution (NO.C3206, Beyotime Biotechnology, China). Briefly, cells were washed 3 times with PBS and fixed with 4% paraformaldehyde solution for 30 min, stained with staining working solution for half an hour, and then washed with PBS to remove residual staining agent. Finally, the blue-violet reaction product was observed with an inverted fluorescence microscope. ALP activity quantitative analysis was performed base on the transformation from p-nitrophenyl phosphate (pNPP) to p-nitrophenyl (pNP) with the presence of ALP using an alkaline phosphatase activity test kit (NO.70-AP0011, MultiSciences, China). Cells seeded as described and cultured for 7, 10, and 14 days were treated according to the manufacturer's instructions with 4 replicates per treatment group. The optical density was read using an ELISA plate reader. The final ALP activity is expressed as enzyme activity/total protein.

Real-time quantitative polymerase chain reaction (RT-qPCR) was used to detect osteogenesis-related genes expression levels of collagen type I (COL-I), osteocalcin (OCN), runt-related transcription factor 2 (Runx-2), alkaline phosphatase (ALP), and bone sialoprotein (BSP) in hBMSCs. Glyceraldehyde phosphate dehydrogenase (GAPDH) was used as a house-keeping gene. The primer sequences of COL-I, OCN, Runx-2, ALP, BSP and GAPDH are shown in Table 1. The cells were cultured in 6-well plates in BRP and BSB osteogenic induction medium (seeding density of 2×10^5 cells per well). 3 replicate samples were prepared for each treatment group. After 7 and 14 days of culturing, total RNA of hBMSCs was extracted using HiPure Total RNA Kit (Magen, China) following the manufacturer's guidelines. The Nanodrop 2000 (Thermo Scientific) spectrophotometer was used to measure total RNA concentration. A cDNA Synthesis Kit (No.D7170 M, BeyoRT™ II, Beyotime Biotechnology, China) was used to perform the RNA reverse transcription. SYBR Green qPCR Mix (NO.D7260, BeyoFast™ II, Beyotime Biotechnology, China) was used for the RT-qPCR reaction. The thermocycle reaction was 30 s of DNA denaturation at 95 °C and 39 cycles of 95 °C for 5 s and 60 °C for 30 s. The melting curve and Ct values were obtained and analyzed using qTOWER3 software (Analytik Jena AG, Germany). Expression levels were calculated based on the difference between the target gene Ct value and the Ct value of DAPDH [$2^{-\Delta Ct}$ where ΔCt = Ct (target gene) – Ct (DAPHD)].

Alizarin Red S (ARS) staining was used to detect the extracellular matrix mineralization of hBMSCs cultured in BSB osteogenic induction medium. After the cells were cultured for 14 days (5×10^4 cells per well in 48-well plate), ARS (Sigma, A5533) was used to stain the calcium nodules formed on the cell surface. Briefly, cells were fixed with 4% paraformaldehyde solution for 30 min and then rinsed with deionized water for 3 times to remove residual formaldehyde solution. The cells were stained with ARS working solution (40 mmol/L, pH = 4.2) for 10 min under shaking, rinsed with deionized water until the residual ARS stain is completely removed. The staining was observed using an inverted fluorescence microscope.

2.6. In-vivo animal experiment

Healthy New Zealand white rabbits from Guangdong Medical Laboratory Animal Center were used to investigate the efficacies of BRPs and BSBs for bone regeneration. All procedures were approved by the animal experimental ethics committee of Guangzhou Medical University.

Six rabbits (3 males and 3 females, average body weight of 2.5 kg, 8 weeks of age) were randomly divided into two groups to investigated

two implantation times, 1 and 3 months. Anesthesia was performed by intravenous injection of sodium pentobarbital (at a dose of 20 mg/kg) to the rabbit's ear vein. The anesthetized rabbit was fixed on the operating table. After depilated and thoroughly disinfected at the surgical area of head, an skin incision about 20 mm length was made on the head, and the subcutaneous tissue, fascia, and periosteum were peeled off layer by layer to expose the skull. Two circular defects 6-mm in diameter were made in the skull at a distance not less than 5 mm apart using an electric drill. The endocranium under the skull was not damaged during the surgery. Bone debris in the skull defects was washed out with sterile normal saline. The front defect was then filled with BRPs (experimental group) and the posterior defect with BSBs (control group). All samples were sterilized using 20 kGy γ-irradiation. Autologous blood was drawn from the rabbit's ear vein for wetting the sterile samples. Samples mixed with blood were filled into the defect site. The front defect site of the skull was filled with BRP, while the posterior defect was filled with the BSB. Barrier membrane, which was commercially available collagen membrane, was used to cover on the particles, with the membrane outer edges extending 2–3 mm beyond the edge of the defect. The periosteum, fascia, and outer skin were then sutured layer by layer and the closed wound was disinfected with 75% alcohol. After the operation, the rabbits were housed individually and penicillin (40 wIU per day) was intramuscularly injected for 3 days as anti-infection treatment. The overall surgical procedure is shown in Fig. 1.

Rabbits were euthanized 1 month and 3 months after surgery, and the bone tissue of the skull defect area was excised, fixed with 10% buffered formalin solution for at least 48 h, and examined as follows. For 3 months implantation samples, a micro computed tomograph (micro-CT) imaging system (XTV160H, X-TEK, UK) was used to scan the microstructure at 60 kV and 67 μA. The scanning data were reconstructed with Materialise Interactive Medical Image Control System (Mimics) software to obtain the 3-dimensional images. For 1 and 3 months implantation samples, after decalcified and embedded in paraffin, samples were cut into slices with thickness of 5 μm at the central part of diameter position using a microtome (RM2016, Leica, Germany). Slices were stained with hematoxylin-eosin (HE) and the stained tissue was observed with optical microscope (DM1000, Leica, Germany).

2.7. Statistical analysis

Data in this study were expressed as means ± standard deviation for all experiments. Treatment group means were compared by Student's t-test. $P < 0.05$ was considered to be statistically significant (*$P < 0.05$, **$P < 0.01$). All photographs were digitally processed using Adobe Photoshop CS.

3. Results

3.1. Phase composition and micromorphology of BRPs and BSBs

Phase compositions of BRPs and BSBs were analyzed by comparing the XRD patterns (Fig. 2) to Joint Committee on Powder Diffraction Standards (JCPDS) cards. Results indicated that the main component of BSB is HA (JCPDS reference code: 00-009-0432), and no secondary phase could be found from the XRD patterns. BRPs were composed mainly of β-tricalcium phosphate (β-$Ca_3(PO_4)_2$ (JCPDS reference code: 00-009-0169). Moreover, the XRD analysis also showed that part of calcium silicate ($CaSiO_3$, JCPDS reference code: 00-001-0720) existed in BRP samples.

Fig. 3 illustrates the micromorphology of BSBs and BRPs. The BSB samples were three-dimensional porous sponge-like structures (Fig. 3A) composed of nano-sized HA particles arranged in a directional order (Fig. 3B). The BRP samples were three-dimensional porous and irregular structures composed mainly of hexagonal crystals ranging in size from 1 to 5 μm with micropores among the crystals (Fig. 3D). Moreover, it seems like that the pores among the crystals were mostly filled with amorphous substances.

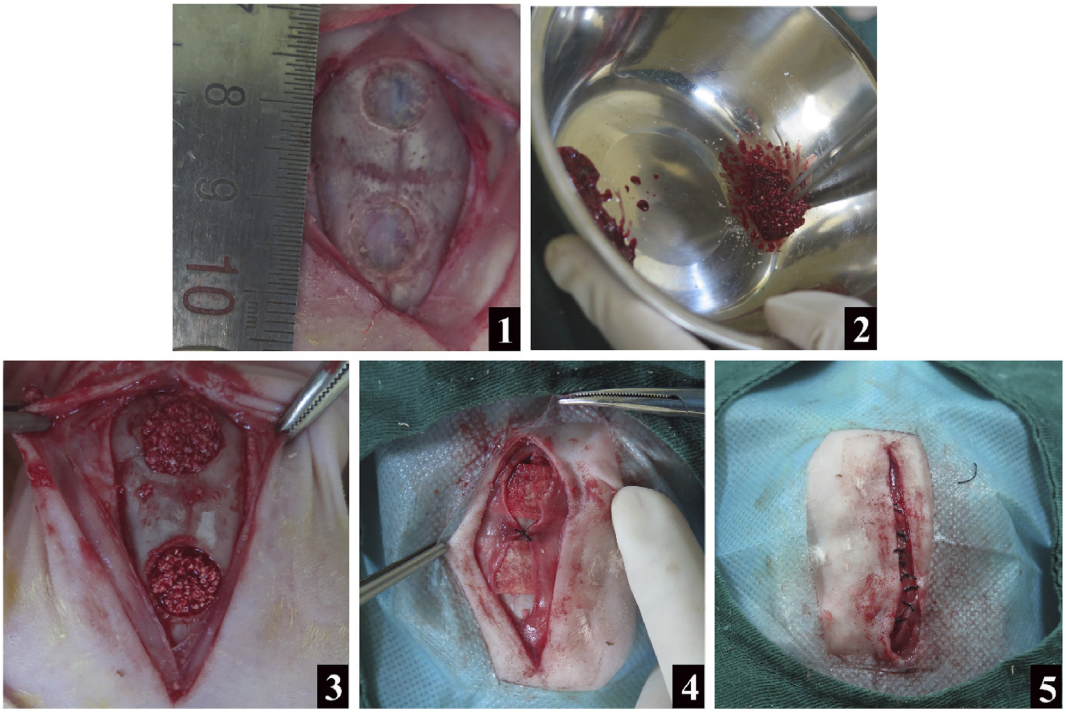

Fig. 1. Rabbit skull defect construction and material implantation for bone regeneration.
1: skull defect construction; 2: mixing of materials (bovine spongy bone or bone regeneration particles) with autologous blood; 3: material implantation; 4: defect covering with a barrier membrane; 5: suturing.

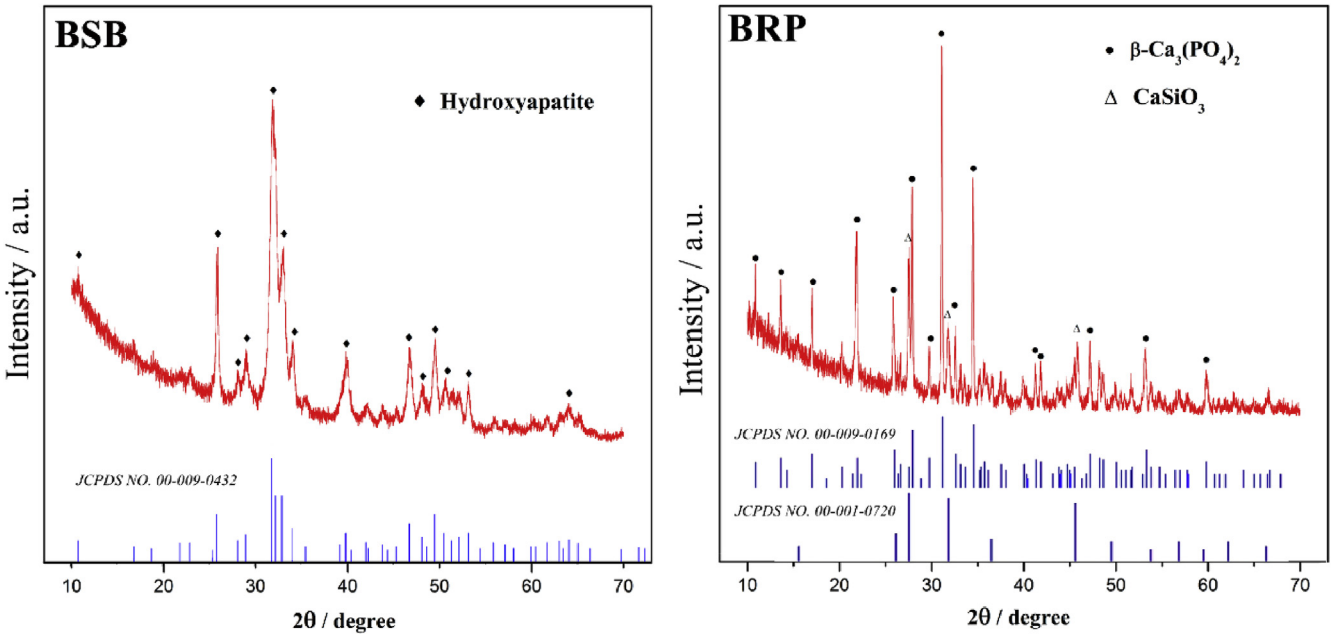

Fig. 2. XRD patterns of BRP and BSB.

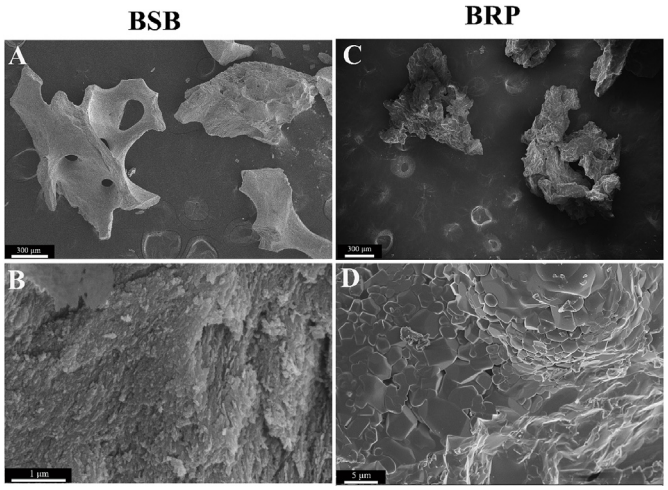

Fig. 3. SEM images of BSB (A and B) and BRP (C and D).

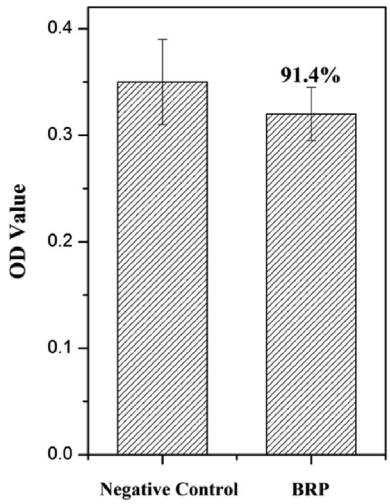

Fig. 4. Cytotoxicity of BRP (repeat number n = 4).

3.2. Cytotoxicity of BRP and the effect of BRP and BSB on the activity of hBMSCs

The result of BRP cytotoxicity assays is shown in Fig. 4. The hBMSCs were cultured for 24 h in the negative control group and BRP extraction. The cell viability was detected by CCK-8. The OD value of the measured result was directly proportional to the number of cells. The results showed that compared with the negative control, the activity of BRP was 91.4% of that in the negative control group. But there's no significantly difference with the result of the negative control, indicating that the BRP material essentially non-toxic (i.e., high biocompatibility). Further, hBMSC number continued to increase over 1, 4, and 7 days in culture with BRPs (Fig. 5) and proliferation was actually higher compared to cells cultured in BSB medium. The OD values after one day were equivalent for BRP and BSBP groups, but were significantly higher in the BRP group on days 3 and 7.

After hBMSCs were cultured in different meida for 2 days, the distribution and activity of cells were tested using Live/Dead staining assay (Fig. 6). The number of living cells (green) was greater in BRP medium than in BSB medium. Moreover, dead cells (red) were more numerous in the BSB group than the BRP group. What's more, most of the cells cultured in BSB medium were not spread and attached well due to their round cell body. However, cells cultured in BRP medium had a better spreading form and cell filopodia could be significantly observed.

3.3. Release behavior of ions from BRP and BSB particles

During hBMSC culture process, the BRP and BSB media were exchange for fresh media every other day and the calcium and silicon ion contents in the removed media were detected using ICP-AES to estimate release rates from BRPs and BSBs (Fig. 7). The free calcium ion content of BRP medium was much higher than that of BSB medium (60–120 ppm vs. 10–20 ppm). Similarly, the Si ion content of BRP medium was between 40 and 55 ppm, while Si was barely detectable in BSB medium. For BRP group, higher amount of Ca and Si ions released at early extraction period than that in the late extraction stage.

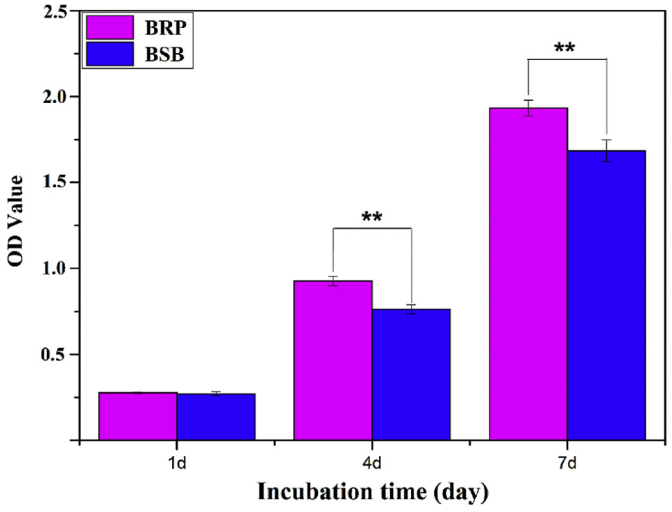

Fig. 5. Proliferation of hBMSCs after incubated in different media for 1, 4, and 7 days (repeat number n = 4).

3.4. Effects of BRP and BSB on osteogenic differentiation of hBMSCs

In the present study, alkaline phosphatase ALP activity, ALP staining, osteogenic differentiation-related gene expression levels (COL-I, Runx-2, ALP, OCN, BSP), and alizarin red staining intensity were measured in hBMSC culture process to compare the osteogenic differentiation capacity of BRPs and BSBs.

The ALP activity of hBMSCs cultured in BRP or BSB medium for 7, 11, and 14 days is shown in Fig. 8. In both groups, ALP activity of hBMSCs increased with the prolongation of culture time. During the whole cell culture period, the ALP activity of the cells for BSB group increased slowly with the prolongation of culture time, and the ALP activity at 14 days did not increase substantially compared with that at 10 days. The BRP group had a significant promotion effect on the increase of ALP activity and its ALP activity had a continuous increase with the prolongation of culture time. At each detection time point, the ALP activity of the cells for BRP group was significant higher than that of the cells for BSB group. The intensity of ALP staining (blue-violet) also increased with time in culture for both groups but was greater at all time points in the BRP group compared to the BSB group, indicating a greater rate ALP secretion from hBMSCs cultured in BRP medium.

Expression levels of the osteogenic-related genes ALP and OCN were also significantly greater in the presence of BRPs than BSBs after 7 days of culture as measured by RT-qPCR (Fig. 9), while after 14 days, expression levels of all measured genes were higher in the BRP group. Finally, alizarin red staining (Fig. 10) was significantly more intense in day-14 hBMSCs cultured in BRP medium, indicating a greater number of calcium nodules formed by extracellular matrix mineralization.

3.5. In-vivo evaluation of BRP and BSB

After the implantation of BRP and BSB materials, New Zealand white rabbits were in good condition after operation, and no deaths occurred. The wounds healed well and there were no abnormal secretions at the wound site. All rabbits could move normally after 12–24 h of recovery after operation.

Hematoxylin-eosin (HE) staining of rabbit skull tissue after 1 M implantation of BRP and BSB is shown in Fig. 11 After 1 M implantation of BRP, there was a certain amount of new bone formation inside the defect, away from the autologous bone. From the 200X picture in Fig. 11 it can be seen that new bone formed around the implanted particles closely, and new woven bones gradually growing into the inner pores of the particles. In addition, nascent vascular tissue was observed. In contrast, the BSB group showed only a small amount of new bone formation at the material-autologous bone interface and on the BSB particle surfaces after one month, but none in the middle of the defect.

After 3 M implantation of BRP and BSB in rabbit skull defects, samples were scanned using micro-CT and then the scanning data were reconstructed into a three-dimensional image for analysis. It can be seen from Fig. 12 the overall bone mineral density of the BRP group defect site is higher than that of the BSBBSB group. The pores among the internal implanted particles of the BRP group had been completely filled by the newly formed bone, leading to a dense overall structure. Alternatively, there were still numerous observable voids among the implanted BSBs, leading to a loose overall structure and poor defect healing. Excellent integration of new bone with ambient natural bone was observed in both groups.

The HE staining images of the rabbit skull tissues implanted with BRP and BSB samples for 3 M are shown in Fig. 13. It can be observed from Fig. 13 that the voids among BRPs were filled with new bone tissue. And along with the biodegradation of BRP, more new bones grew into the inner pores of particles. Compared to implants after one month, both the size and connection of the trabecular bone were increased. After 3 M implantation, the BSB group exhibited little new bone formation in the middle of the defect on the side close to the dura mater. Although there was a small amount of new bone growing around the BSB particles in other areas, most of the voids among the particles were not filled with new bone.

4. Discussion

β-TCP has long been utilized as bone substitution material or as an additive to other matrix materials due to its demonstrated bioactivity and biodegradability [20]. However, its clinical utility is still limited by low osteoinductivity. Si-containing materials are attractive alternatives for bone regeneration as Si release can promote osteogenesis and apatite formation [21]. In the present study, we developed bone regeneration particles (BRPs) by sintered the mixture of amorphous calcium phosphate (ACP) as the apatite source and 58S bioglass powder as

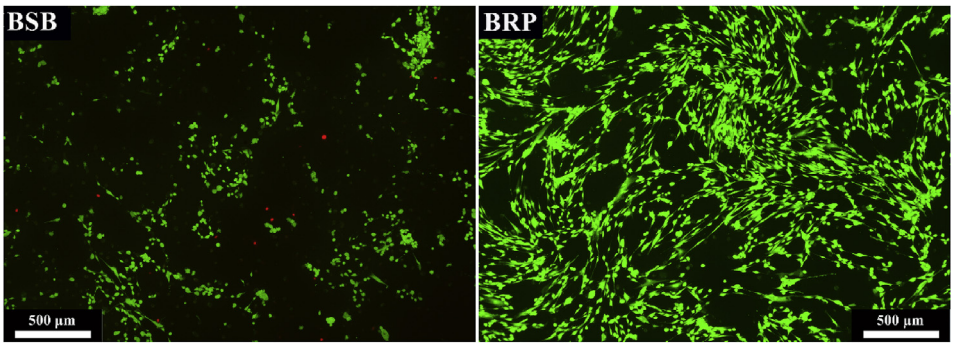

Fig. 6. Live/dead fluorescence staining images of hBMSCs after cultured in different meida for 2 days.

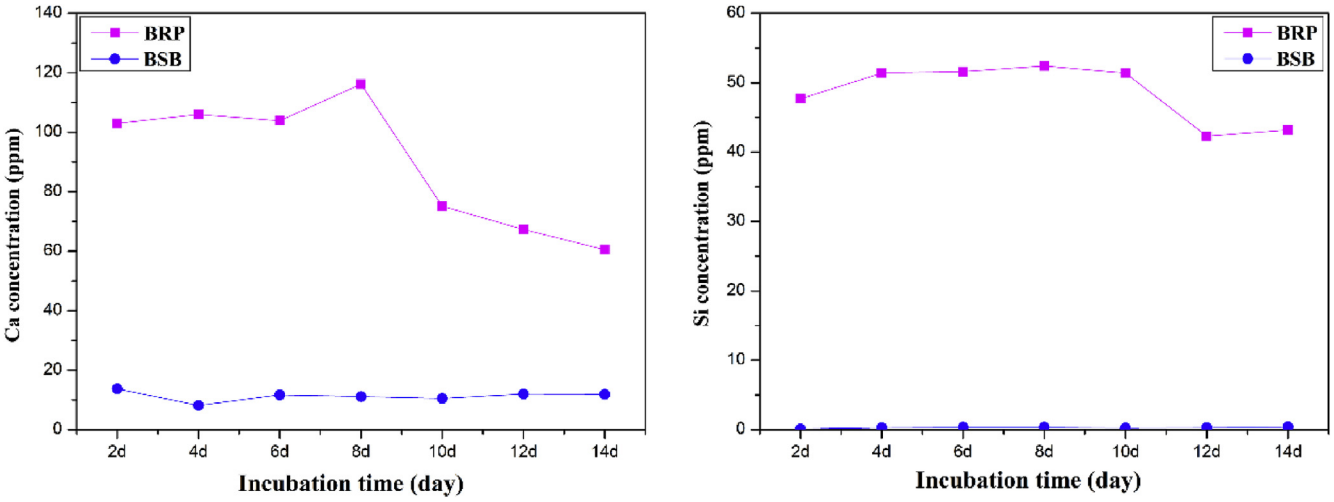

Fig. 7. Ca and Si concentrations in BRP and BSB meida respectively during cell culture process (repeat number n = 3).

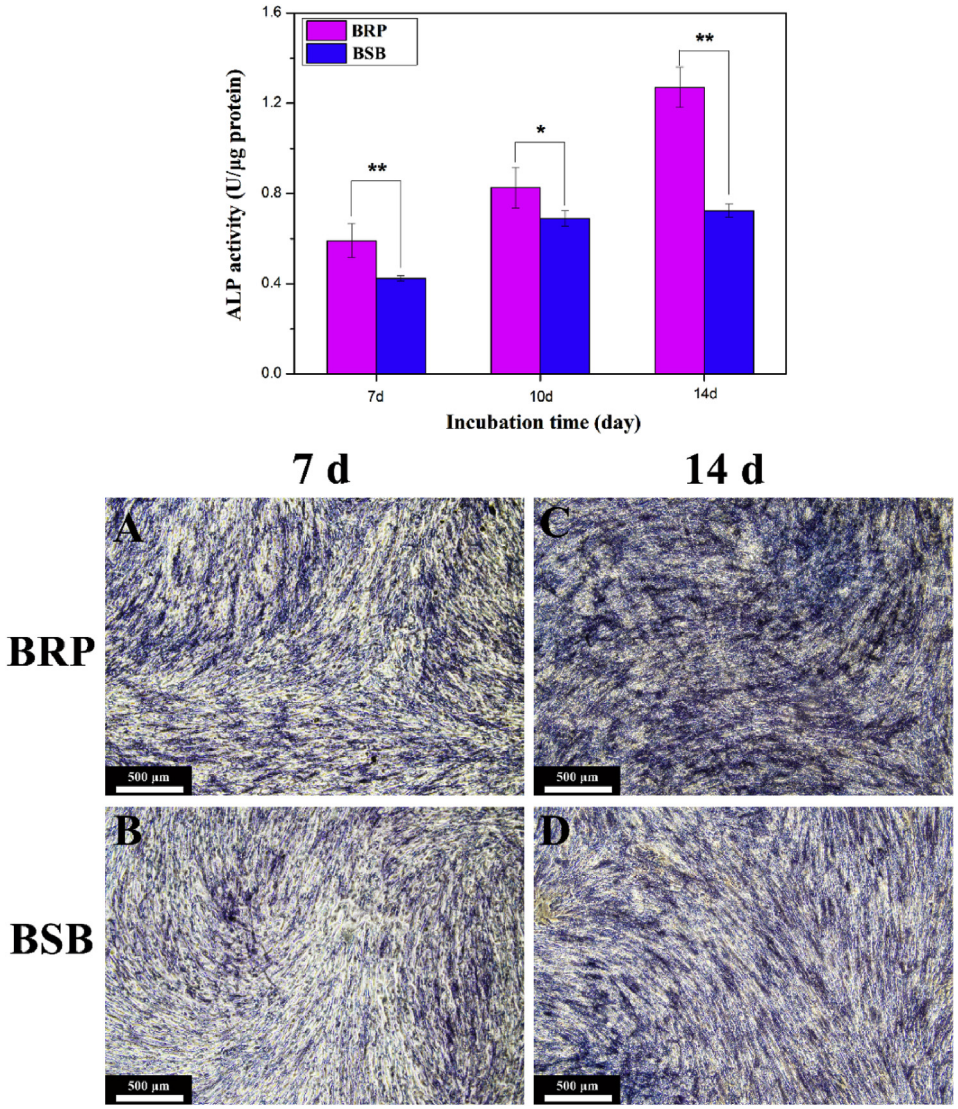

Fig. 8. ALP activity quantitative analysis and ALP staining of hBMSCs after incubated in different soaking extractions for 7, 10, and 14 days (repeat number n = 4).

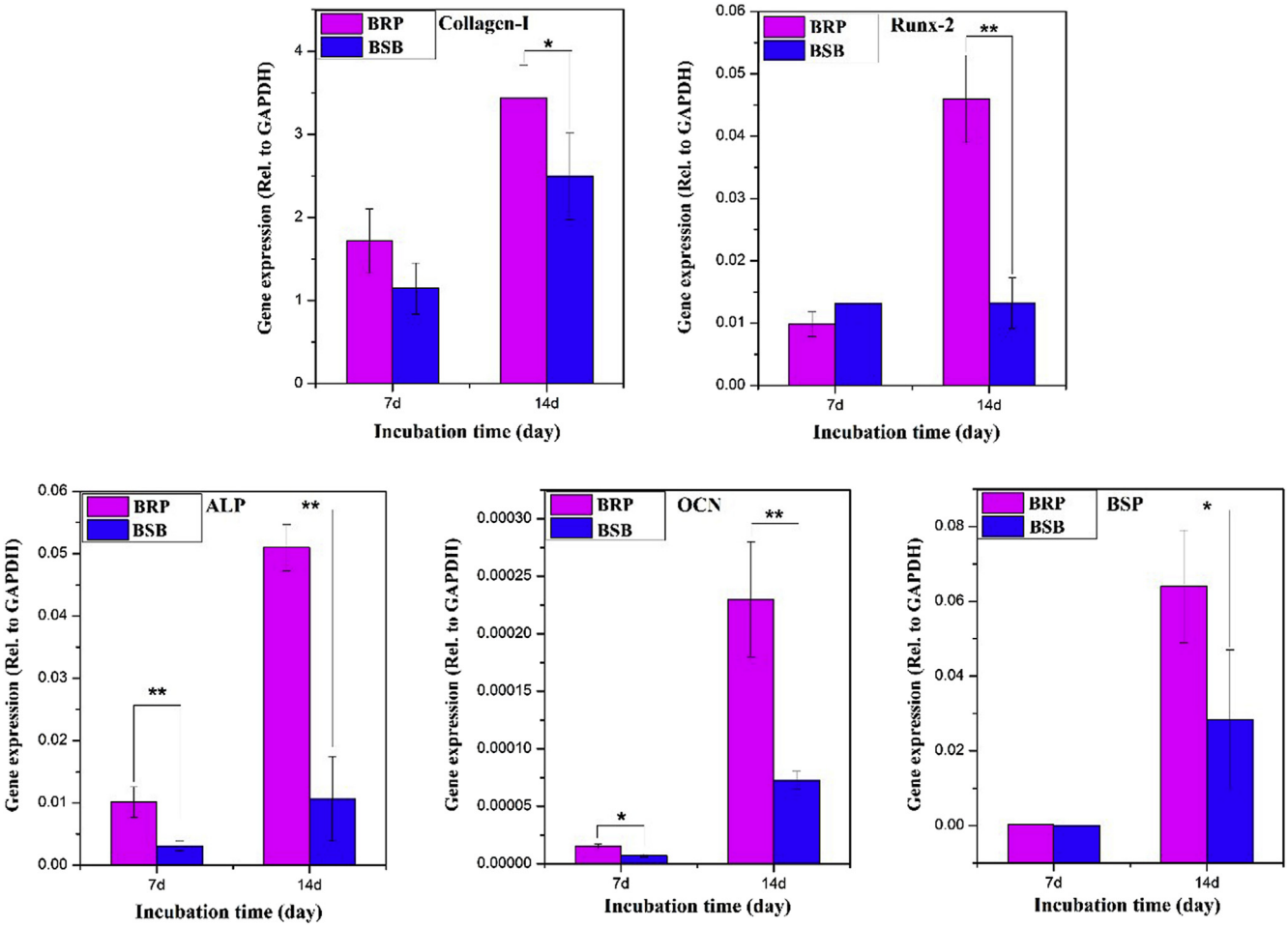

Fig. 9. The expression of osteogenic-genes COL-I, Runx-2, ALP, OCN and BSP from hBMSCs cultured for 7 and 14 days (repeat number n = 3).

the Si source. Commercially available bovine spongy bone (BSB) was used as control group to help understand the biological properties and osteogenic availability of BRP. The main component of BSB is HA, which was obtained by processing bovine spongy bone and didn't contain any organic components, resulting in relatively slow degradation rate after implantation into natural bone defects. It can be seen from the analysis of Fig. 2 that BRP was composed of β-TCP and $CaSiO_3$. During the heat treatment process, the crystallinity of amorphous calcium phosphate gradually increased, and finally tricalcium phosphate phase formed due to the Ca/P ratio was 1.5. ACP and 58S powders were sintered at 1250 °C, which was a relatively higher heat treatment temperature. During the sintering process, $CaSiO_3$ appeared due to the crystallization of 58S, forming a glass ceramic, which is in accordance with previous report that $CaSiO_3$ content increased gradually after 58S being sintered at 1000 °C and 1200 °C [22].

Surface topography analysis of BRP and BSB was performed in the experiment. BSB was derived from natural cancellous bone, so it was three-dimensional porous sponge-like structure with orderly arranged nano-sized HA particles, which is exactly the crystal arrangement of natural bone [23]. BRP was also a three-dimensional porous irregular particle. From the enlarged view, the crystal was mainly hexagonal, with size between 1 μm and 5 μm, and some micropores existed among the crystals. Moreover, it seems like that the areas among the crystals were mostly filled with amorphous substances. This structural feature may be caused by the liquefaction of the bioglass during the sintering process. Bioglass had relatively lower melting temperature [24], and

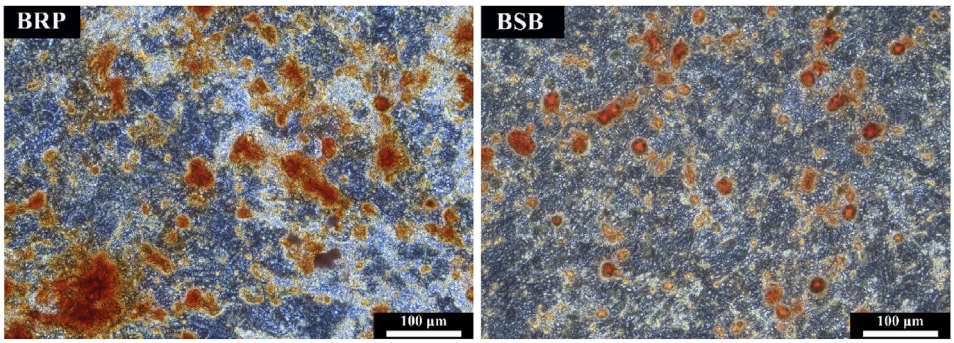

Fig. 10. Alizarin Red S (ARS) staining pictures of hBMSCs cultured for 21 days. (For interpretation of the references to color in this figure legend, the reader is referred to the Web version of this article.)

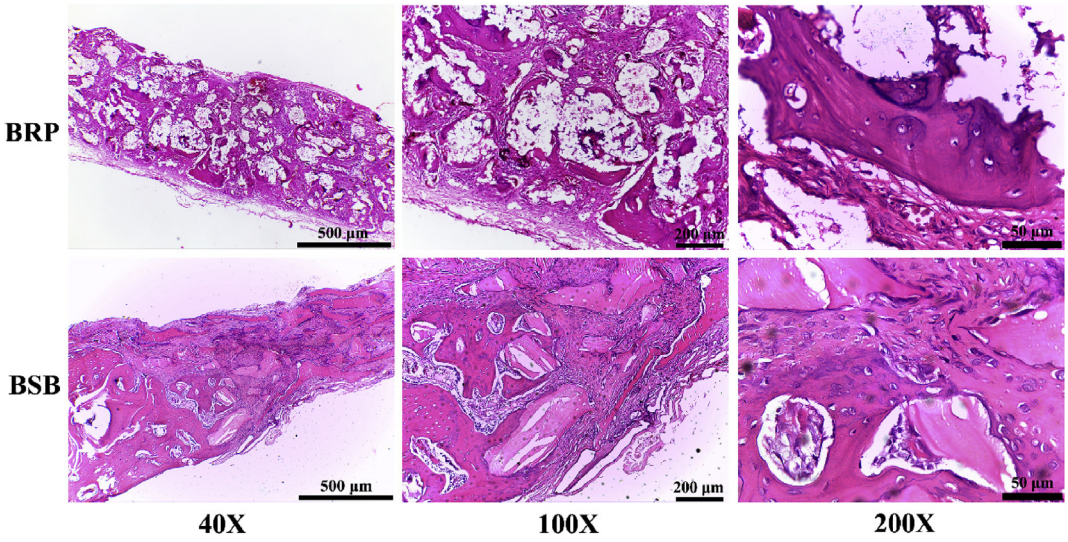

Fig. 11. Histological examination (HE staining) of skull bone defects in rabbits after the implantation of BRP and BSB for 1 month.

bioglass in the molten state may flow into the pores between granules. It has been reported that, many studies were carried out by adding bioglass into hydroxyapatite scaffold to repair the cracks of the porous scaffold that were formed during sintering process. Molten bioglass could fill the cracks of the scaffold, so that the strength of the scaffold was greatly improved [25,26].

The cytotoxicity of BRPs was tested according to ISO 10993-5. As shown in Fig. 4, the OD value of hBMSCs cultured in BRP soaking solutions was no significant difference with that of the negative control, indicating that the BRP material was not cytotoxic. However, the results showed that the activity of BRP was 91.4% of that in the negative control group. When the BRP samples soaked in culture medium, a certain amount of Si ions will be released, resulting in an alkaline environment [27]. Thus, these BRPs appear to be essentially non-toxic against osteogenic cells. In addition, these particles in culture medium demonstrated relatively stable Si and Ca release behavior and greater total release rate compare to BSBs in medium (Fig. 7). The ion content in the solution detected in the experiment was the total content released within every two days. Due to the different solubility of the chemical composition of the materials, the content of calcium ions and silicon ions in the BRP soaking solution was higher, while the content of calcium ions in the BSB soaking solution was relatively lower. In fact, almost no silicon was detected in the BSB medium, although the natural bone contains silicon element. In the BRP medium, the ion content in the early extraction period was slightly higher than in the late extraction stage. The release content of ions from BRP decreased at later stage of soaking, possibly due to the reprecipitation of apatite on the surface of samples, which would inhibit further Ca and Si release. Nonetheless, the enhanced release was manifested by greater osteoinductivity and extracellular matrix mineralization.

In addition to good biocompatibility, the BRPs also promoted greater cell proliferation compared to BSBs (Fig. 5). The amount of cells and cell proliferation rate of BRP group were significantly higher than those of BSB group, and there were significant differences in the amount of cells between the two groups. The cells uniformly distributed on cell culture flasks remained good activity after 2 days incubation in soaking solutions. Cells cultured in BRP solutions had greater amount, higher cell activity, and better spreading morphology than those of BSB group. Studies have shown that the silicon ions with appropriate concentration have a significant effect on cell growth. In the ES Thian study, HOBs showed a faster rate of proliferation and higher ability to extracellular matrix mineralization on Si-HA coatings compared to pure HA coatings [28]. Also SEM observation showed well hMSCs adhesion and spreading on Si-containing materials surface [29]. And some studies have shown that the Si-containing apatite biomaterials can also prevent any cell damage caused by external environmental changes [30]. Therefore, the greater Si release capacity of BRPs may account for the substantially better bioactivity, including osteoconductive function, compared to BSBs.

Since the material is irregularly granulated, cell adhesion is not easy to evaluate, so the adhesion of hBMSCs on the surface of the material was not detected in this experiment. But the BRP material contains Si

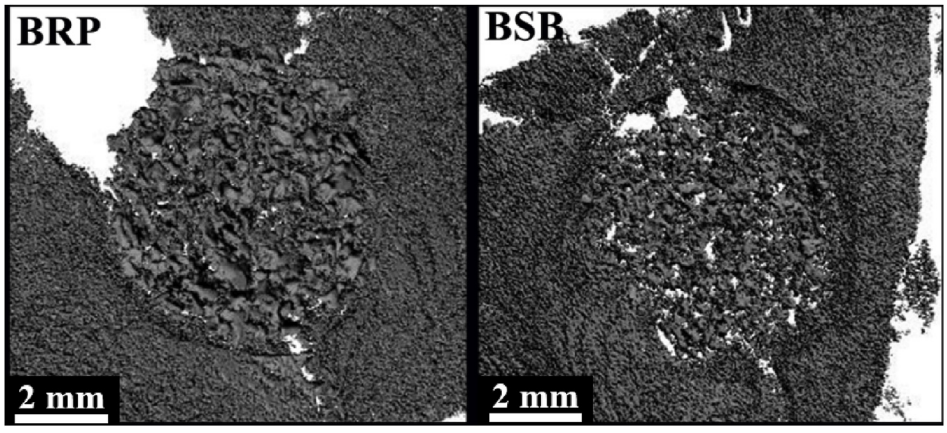

Fig. 12. Micro-CT three dimensional reconstruction images of rabbit skull bone defects after the implantation of BRP and BSB for 3 months.

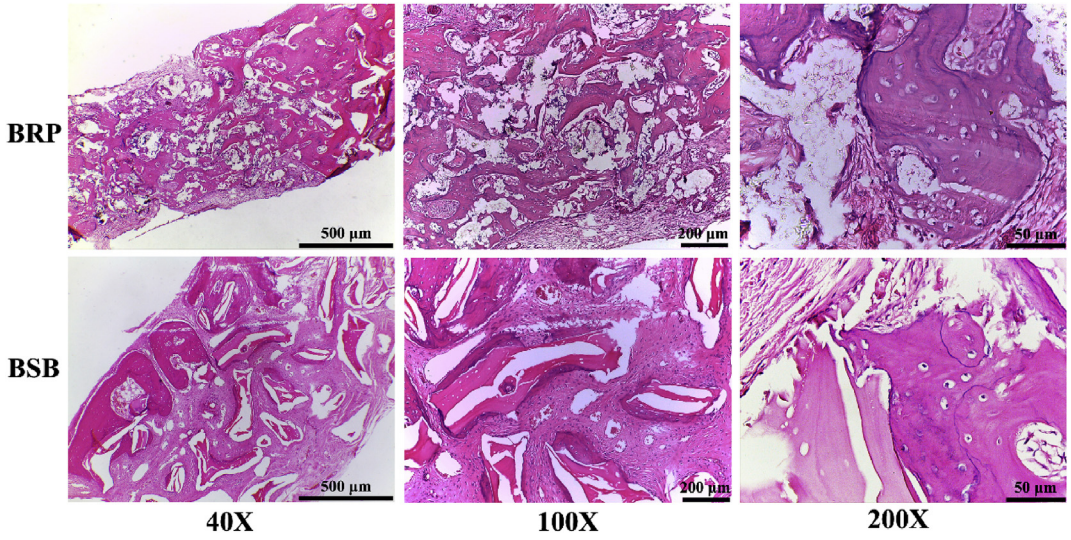

Fig. 13. Istological examination (HE stain) of skull bone defects of rabbits after the implantation of BRP and BSB for 3 month.

element, and the silicon released from the material usually combined with the oxygen atom and was able to form a silicon oxygen network structure in the material. This structure can bind to metal elements in proteins, thereby promoting the adsorption of proteins on the surface of the material [31]. In turn, the proteins adsorbed on the surface of the material can interact with integrins on the cell surface to mediate better cell-substrate adhesion [32]. Therefore, we speculated that BRP material would have excellent osteoconduction function after implantation into natural bone by promoting the adhesion and migration of osteoblasts, resulting in better interface bonding and osteointegration. Previous studies have also reported that silicate ions released from silicon-containing materials have an adhesion-enhancing effect. Thian et al. found that cells can spread better on Si-HA coatings than on pure HA coatings, and immunofluorescence staining revealed a large amount of visible actin filament formation in the cytoplasm on Si-containing coatings [32]. In addition, Si-containing HA promoted adhesion of human osteoblasts (HOBs) on the surface of the material [33].

Osteogenic differentiation was also enhanced by BRPs compared to BSBPs as evidenced by greater ALP activity, ALP staining, expression of osteogenic differentiation-related genes (COL-I, Runx-2, ALP, OCN, BSP), and alizarin red staining. Under the osteogenic stimulation of the external environment, hBMSCs will enter into the stage of osteogenic differentiation accompanied by the maturation and mineralization of the extracellular matrix. ALP is one of the markers of early differentiation of cells, which is secreted during the maturity of extracellular matrix and promotes the mineralization of matrix in the later stage [34]. In this experiment, the ALP activity of hBMSCs cultured in BRP and BSB soaking solutions was studied by quantitative analysis and qualitative analysis. The BRP group has a significant promotion effect on the increase of ALP activity. It can also be seen from the ALP staining experiment that the blue-purple color of BRP group cells was deeper than that of BSB group, indicating that the amount of ALP secreted by cells in BRP group was higher than that in BSB group. Silicon ions have a certain promoting effect on the improvement of ALP activity. Studies by CM Botelho et al. reported that Si increased ALP activity and total protein content in osteoblasts in vitro [35]. Thus, the enhanced ALP activity in hBMSCs cultured in BRPs likely also stemmed for greater Si release.

Human BMSCs cultured in BRP medium also generated greater numbers of calcium nodules via extracellular matrix mineralization than cells grown in BSBP medium. Again, this was likely due to the greater supply of calcium and silicon ions released from BRP samples. Indeed, a previous study demonstrated that calcium silicate compounds induced osteo-like apatite formation [36]. Compared to BSBs, BRPs also enhanced expression of osteogenic genes as evidenced by RT-qPCR. COL-I is the main component of extracellular matrix collagen, and COL-I is also one of the marker genes expressed in early stage of osteogenic differentiation. As a specific bone transcription factor, Runx-2 plays an important role in new bone formation by promoting gene transcription during osteogenic differentiation [37]. BSP is a bone-specific calcium-binding glycoprotein that promotes apatite nucleation, calcium binding, and nodule formation [29,38]. Finally, OCN is expressed in late stages of osteogenic differentiation and is also closely related to the mineralization of extracellular matrix. Runx-2 can also indirectly promote the mineralization of extracellular matrix [39]. Further, silicate-containing calcium phosphate bioceramics can activate the Wnt/β-catenin signaling pathway, which plays an important role in osteogenic differentiation [40,41], and this pathway may be activated due to the release of Ca and Si [42,43]. Therefore, the relevant indicators related to mineralization and the expression level of osteogenic genes were up-regulated, which was closely related to the induction effect of silicon. To sum up, BRP has better osteogenic induction performance than BSB particles.

Finally, the superior osteoinductivity of BRP was directly demonstrated in a rabbit skull defect model. New bone grew around the BRP samples, and some new bones grew into the pores of the particles as the degradation of BRP. New bone formed at both the middle and the edge of the defect, indicating that the new bone grew under both bone conduction and osteoinduction mechanisms after BRP implantation. The construction and formation of new blood vessel is the key to the success of tissue repair. After implantation, there were many capillaries in the defect area, indicating that new blood circulation system was gradually formed during the repair of new bone tissue, thereby ensuring transportation of oxygen and nutrients and excretion of tissue metabolites in the new bone area. After 3 M implantation of BRP material, the gap between the particles has been basically filled by the new bone, meaning a successful bone regeneration result. After one month after BSB implantation, most of the new bone was wrapped around the BSB particles, and there was no new bone found in the middle of the defect. Three months after implantation of BRPs, however, the gap between the particles had been filled by new bone, while there were still voids among BSB particles, leading to a loose overall structure and poor defect healing. Bone defect was repaired only through the bone conduction mechanism for BSB particles. Further, fewer capillaries were observed in BSB-treated defects, limiting nutrient supply for growth. While both groups showed good interface bonding at 3 months after implantation, the presence of Si in the BRPs appears to have enhanced osteogenic activity, resulting in a higher bone regeneration rate.

5. Conclusion

ACP and 58S powders were used as raw materials to synthesize novel bone regeneration particles (BRPs). A porous block precursor was prepared by lyophilization and the final bioactive bone particles were obtained through fragmentation and heat treatment. Commercially available bovine spongy bone without organic components was selected as the control material for comparison. XRD and SEM analysis showed that BRP was composed of β-TCP and calcium silicate with a microstructure formed by hexagonal 1–5 μm crystals, while BSBPs were mainly composed of orderly arranged nano-sized HA crystals. In vitro cell experiments showed that BRPs were non-toxic to human bone mesenchymal stem cells (hBMSCs) and that hBMSC proliferated faster in BRP-containing medium than BSB-containing medium. The regulated ALP activity, alizarin red staining, and the expression level of osteogenic-related genes of BRP group indicating its superior osteoinductivity compared to BSB. Silicon ions were dissolved stably from BRP samples during cell culture period, which played crucial roles in cell biological function. BRP and BSBs. The BRPs also showed greater bone repair efficacy in a rabbit skull bone defect model through HE staining and micro-CT analysis. Thus, BRP demonstrated superior osteoconduction and osteoinduction properties compared to BSBPs and so may hold great promise for alveolar bone repair surgery.

Acknowledgements

This research was supported by the Special Project of International Scientific and Technological Cooperation in Guangzhou Development District under Grant No. 2017GH19 and Project of Guangdong Provincial Health Department under Grant No. A2014566.

References

[1] G.O. Shabestari, Y.S. Shayesteh, A. Khojasteh, et al., Implant placement in patients with oral bisphosphonate therapy: a case series, Clin. Implant Dent. Relat. Res. 12 (2010) 175–180 https://doi.org/10.1111/j.1708-8208.2009.00150.x.

[2] A. Khojasteh, H. Behnia, Y.S. Shayesteh, et al., Localized bone augmentation with cortical bone blocks tented over different particulate bone substitutes: a retrospective study, Int. J. Oral Maxillofac. Implant. 27 (6) (2012) 1481–1493 https://doi.org/10.1016/j.stomax.2011.12.016.

[3] R. Kolerman, J. Nissan, H. Tal, Combined osteotome-induced ridge expansion and guided bone regeneration simultaneous with implant placement: a biometric study, Clin. Implant Dent. Relat. Res. 16 (5) (2014) 691–704 https://doi.org/10.1111/cid.12041.

[4] M. Viswambaran, V. Arora, R.C. Tripathi, et al., Clinical evaluation of immediate implants using different types of bone augmentation materials, Med. J. Armed Forces India 70 (2) (2014) 154–162 https://doi.org/10.1016/j.mjafi.2012.04.020.

[5] W. Becker, B.E. Becker, R. Caffesse, A comparison of demineralized freeze-dried bone and autologous bone to induce bone formation in human extraction sockets, J. Periodontol. 65 (12) (1994) 1128–1133 https://doi.org/10.1902/jop.1994.65.12.1128.

[6] A. Barone, Aldini, Nicolò Nicoli, M. Fini, et al., Xenograft versus extraction alone for ridge preservation after tooth removal: a clinical and histomorphometric study, J. Periodontol. 79 (8) (2008) 1370–1377 https://doi.org/10.1902/jop.2008.070628.

[7] C. Luigi, P. Gaia, C. Elena, et al., Alveolar socket preservation technique: effect of biomaterial on bone regenerative pattern, Ann. Anat. 206 (2016) 73–79 https://doi.org/10.1016/j.aanat.2015.05.007.

[8] I.A. Urban, H. Nagursky, J.L. Lozada, et al., Horizontal ridge augmentation with a collagen membrane and a combination of particulated autogenous bone and anorganic bovine bone-derived mineral: a prospective case series in 25 patients, Int. J. Periodontics Restor. Dent. 33 (3) (2013) 299–307 https://doi.org/10.11607/prd.1407.

[9] W. Ozaki, S.R. Buchman, Volume maintenance of onlay bone grafts in the craniofacial skeleton: micro-architecture versus embryologic origin, Plast. Reconstr. Surg. 102 (1998) 291–299 https://doi.org/10.1192/bjp.bp.106.024026.

[10] G. Widmark, B. Andersson, C.J. Ivanoff, Mandibular bone graft in the anterior maxilla for single-tooth implants. Presentation of surgical method, Int. J. Oral Maxillofac. Surg. 26 (1997) 106–109 https://doi.org/10.1016/S0901-5027(05)80827-6.

[11] J.M. Bouler, P. Pilet, O. Gauthier, et al., Biphasic calcium phosphate ceramics for bone reconstruction: a review of biological response, Acta Biomater. 53 (2017) 1–12 https://doi.org/10.1016/j.actbio.2017.01.076.

[12] M. Arora, E. Arora, The promise of silicon: bone regeneration and increased bone density, J. Arthrosc. Joint Surg. 4 (3) (2017) 103–105 https://doi.org/10.1016/j.jajs.2017.10.003.

[13] A.F. Khan, M. Saleem, A. Afzal, et al., Bioactive behavior of silicon substituted calcium phosphate based bioceramics for bone regeneration, Mater. Sci. Eng. C 35 (2014) 245–252 https://doi.org/10.1016/j.msec.2013.11.013.

[14] X. Wang, A. Ito, X. Li, et al., Signal molecules-calcium phosphate coprecipitation and its biomedical application as a functional coating, Biofabrication 3 (2011) 022001https://doi.org/10.1088/1758-5082/3/2/022001.

[15] X. Wang, A. Ito, Y. Sogo, et al., Silicate-apatite composite layers on external fixation rods and in vitro evaluation using fibroblast and osteoblast, J. Biomed. Mater. Res. A 92 (3) (2010) 1181–1189 https://doi.org/10.1002/jbm.a.32436.

[16] L.L. Hench, The story of bioglass: from concept to clinic, Imp. Coll. Inaugural Lect. Mater. Sci. Mater. Eng. (2015), https://doi.org/10.1142/9781848161740_0006.

[17] P. Sepulveda, J.R. Jones, L.L. Hench, Characterization of melt-derived 45S5 and sol-gel-derived 58S bioactive glasses, J. Biomed. Mater. Res. 58 (6) (2001) 734–740 https://doi.org/10.1002/jbm.10026.

[18] L.L. Hench, H.A. Paschall, Direct chemical bond of bioactive glass-ceramic materials to bone and muscle, J. Biomed. Mater. Res. 7 (3) (1973) 25–42 https://doi.org/10.1002/jbm.820070304.

[19] T. Livingston, P. Ducheyne, J. Garino, In vivo evaluation of a bioactive scaffold for bone tissue engineering, J. Biomed. Mater. Res. 62 (1) (2002) 1–13 https://doi.org/10.1002/jbm.10157.

[20] J. Zhang, H. Wu, F. He, et al., Concentration-dependent osteogenic and angiogenic biological performances of calcium phosphate cement modified with copper ions, Mater. Sci. Eng. C 99 (2019) 1199–1212.

[21] G. Maria, Z. Fausto, D.E. Micaela, et al., Highly porous polycaprolactone scaffolds doped with calcium silicate and dicalcium phosphate dihydrate designed for bone regeneration, Mater. Sci. Eng. C 102 (2019) 341–361.

[22] J. Ma, C.Z. Chen, D.G. Wang, et al., Influence of the sintering temperature on the structural feature and bioactivity of sol-gel derived SiO_2-CaO-P_2O5 bioglass, Ceram. Int. 36 (6) (2010) 1911–1916 https://doi.org/10.1016/j.ceramint.2010.03.017.

[23] S. Weiner, H.D. Wagner, The material bone: structure-mechanical function relations, Annu. Rev. Mater. Res. 28 (1) (2003) 271–298 https://doi.org/10.1146/annurev.matsci.28.1.271.

[24] A.A. El-Rashidy, J.A. Roether, L. Harhaus, et al., Regenerating bone with bioactive glass scaffolds: a review of, in vivo, studies in bone defect models, Acta Biomater. 62 (2017) 1–28 https://doi.org/10.1016/j.actbio.2017.08.030.

[25] J.D. Santos, R.L. Reis, F.J. Monteiro, et al., Liquid phase sintering of hydroxyapatite by phosphate and silicate glass additions: structure and properties of the composites, J. Mater. Sci. Mater. Med. 6 (1995) 348–352 https://doi.org/10.1007/BF00120303.

[26] J.C. Knowles, W. Bonfield, Development of a glass reinforced hydroxyapatite with enhanced mechanical properties. The effect of glass composition on mechanical properties and its relationship to phase changes, J. Biomed. Mater. Res. 27 (1993) 1591–1598 https://doi.org/10.1002/jbm.820271217.

[27] K. Xiong, J. Zhang, H. Shi, et al., Preparation and in vitro cell-biological performance of sodium alginate/nano-zinc silicate co-modified calcium silicate bioceramics, RSC Adv. 5 (11) (2015) 8329–8339 https://doi.org/10.1039/c4ra15128c.

[28] E.S. Thian, J. Huang, S.M. Best, et al., Silicon-substituted hydroxyapatite: the next generation of bioactive coatings, Mater. Sci. Eng. C 27 (2) (2007) 251–256 https://doi.org/10.1016/j.msec.2006.05.016.

[29] M. Sepantafar, H. Mohammadi, R. Maheronnaghsh, et al., Single phased silicate-containing calcium phosphate bioceramics: promising biomaterials for periodontal repair, Ceram. Int. 44 (10) (2018) 11003–11012 https://doi.org/10.1016/j.ceramint.2018.03.050.

[30] D. Arcos, S. Sánchez-Salcedo, I. Izquierdo-Barba, et al., Crystallochemistry, textural properties, and in vitro biocompatibility of different silicon-doped calcium phosphates, J. Biomed. Mater. Res. A 78 (4) (2006) 762–771 https://doi.org/10.1002/jbm.a.30790.

[31] K. Schwarz, Proceedings: recent dietary trace element research, exemplified by tin, fluorone, and silicon, Fed. Proc. 33 (6) (1974) 1748–1757.

[32] E.S. Thian, J. Huang, S.M. Best, et al., The response of osteoblasts to nanocrystalline silicon-substituted hydroxyapatite thin films, Biomaterials 27 (13) (2006) 2692–2698 https://doi.org/10.1016/j.biomaterials.2005.12.019.

[33] S. Zou, D. Ireland, R.A. Brooks, et al., The effects of silicate ions on human osteoblast adhesion, proliferation, and differentiation, J. Biomed. Mater. Res. B 90 (1) (2009) 123–130 https://doi.org/10.1002/jbm.b.31262.

[34] S.G. Stein, B.J. Lian, G.L. Gerstenfeld, et al., The onset and progression of osteoblast differentiation is functionally related to cellular proliferation, Connect. Tissue Res. 20 (1–4) (1989) 3–13 https://doi.org/10.3109/03008208909023869.

[35] C.M. Botelho, R.A. Brooks, S.M. Best, et al., Human osteoblast response to silicon-substituted hydroxyapatite, J. Biomed. Mater. Res. A 79A (3) (2006) 723–730 https://doi.org/10.1002/jbm.a.30806.

[36] A. Oryan, S. Alidadi, Reconstruction of Radial Bone Defect in Rat by Calcium Silicate Biomaterials, Life Sciences, 2018 S0024320518301620 https://doi.org/10.1016/j.lfs.2018.03.048.

[37] T. Komori, Regulation of osteoblast differentiation by transcription factors, J. Cell. Biochem. 99 (5) (2006) 1233–1239 https://doi.org/10.1002/jcb.20958.

[38] J.A.R. Gordon, C.E. Tye, A.V. Sampaio, et al., Bone sialoprotein expression enhances osteoblast differentiation and matrix mineralization in vitro, Bone 41 (2007) 462–473 https://doi.org/10.1016/j.bone.2007.04.191.

[39] Marlène Elias, C. Potvin, Cell-type-dependent up-regulation of in vitro mineralization after overexpression of the osteoblast-specific transcription factor Runx2/Cbfal, J. Bone Miner. Res. 17 (11) (2002) 1931–1944 https://doi.org/10.1359/jbmr.2002.17.11.1931.

[40] V. Krishnan, H.U. Bryant, O.A. Macdougald, Regulation of bone mass by Wnt signaling, J. Clin. Investig. 116 (5) (2006) 1202–1209 https://doi.org/10.1172/

JCI28551.1202.
[41] D. Zhai, M. Xu, L. Liu, et al., Silicate-based bioceramics regulating osteoblast differentiation through a BMP2 signalling pathway, J. Mater. Chem. (5) (2017) 7297–7306 https://doi.org/10.1039/C7TB01931A.
[42] J. Bolander, Y.C. Chai, L. Geris, et al., Early BMP, Wnt and Ca^{2+}/PKC pathway activation predicts the bone forming capacity of periosteal cells in combination with calcium phosphates, Biomaterials 86 (2016) 106–118 https://doi.org/10.1016/j.biomaterials.2016.01.059.
[43] J. Costa-Rodrigues, S. Reis, A. Castro, et al., Bone anabolic effects of soluble Si: in vitro studies with human mesenchymal stem cells and CD14+ osteoclast precursors, Stem Cell. Int. (2) (2016) 5653275 https://doi.org/10.1155/2016/5653275.